GROUND-PENETRATING RADAR INVESTIGATION OF SALVAGED TIMBER GIRDERS FROM BRIDGES ALONG ROUTE 66 IN CALIFORNIA[1]

Xi Wu
PhD Student
School of IoT Engineering
Jiangnan University
Wuxi, China
E-mail: xw20170909@gmail.com

*Christopher Adam Senalik**†*
Research General Engineer
E-mail: christopher.a.senalik@usda.gov

James P. Wacker
Research General Engineer
E-mail: james.p.wacker@usda.gov

Xiping Wang†
Research Forest Products Technologist
USDA Forest Service
Forest Products Laboratory
Madison, WI
E-mail: xiping.wang@usda.gov

*Guanghui Li**
Professor
School of IoT Engineering
Jiangnan University
Wuxi, China
E-mail: ghli@jiangnan.edu.cn

(Received July 2019)

Abstract. This study describes assessment of the internal conditions of timber bridge structural members along Route 66 in California. These timber bridges were exposed to desert climate conditions for several decades, which can lead to a variety of deterioration. Overtime, the deterioration may cause loss of structural integrity within the bridges and lead to potentially hazardous conditions for the motoring public. Members from dismantled bridges were brought to the Forest Products laboratory in Madison, WI. Strength-reducing features including decay, splits and cracks, insect attack, and corrosion of metal components were initially identified using visual inspection. Further assessment was then performed using several nondestructive testing technologies including ground-penetrating radar (GPR). GPR was used, among other nondestructive techniques, to identify and locate internal features and defects within the timbers. The tomographic output of the GPR, known as radargrams, revealed deterioration. Based on the information contained within the radargrams, it was possible to classify some internal features and defects with a high degree of certainty, whereas others remained less clear. In this study, the potential of using GPR for inspection of bridge timbers is discussed and supported through interpretation of the radargrams.

Keywords: Ground-penetrating radar, timber bridge, steel nail, hole, decay, split.

* Corresponding author
† SWST member
[1] This article was written and prepared by US Government employees on official time, and it is therefore in the public domain and not subject to copyright.

Wood and Fiber Science, 52(1), 2020, pp. 73-86
https://doi.org/10.22382/wfs-2020-007

INTRODUCTION

Nondestructive testing (NDT) techniques are important methods to assess the internal condition of wood structures. They provide reliable means of determining damage to the timber without compromising the structural performance. Several NDT methods were used in this study for internal inspection of historical bridge timbers, including acoustic wave, radar wave, ultrasonic, and microdrilling. This study mainly addresses the results of the radar wave test.

Ground- penetrating radar (GPR) technology has been used for more than 30 yr for inspecting internal features of materials. The technique has two key positive aspects: data acquisition is rapid and the output is viewable using high-resolution imaging capabilities (Novo et al 2014; Núñez-Nieto et al 2014). GPR is a geophysical method that uses an antenna to generate short bursts of electromagnetic energy in solid materials. Waveforms are transmitted into the structure using an antenna positioned at the surface. The two-way travel time and amplitude of reflected waves are recorded and used to generate the output images. The incident wave propagates through the material and partially reflects at interfaces, presenting a dielectric contrast. When radar pulses encounter a boundary with differing dielectric properties, the electromagnetic waves reflect, refract, and/or diffract from the boundary in a predictable manner. The electromagnetic response of the structure, consisting of all the reflected waves, is then recorded, processed, and analyzed to measure the travel time, propagation velocities, and amplitude of the direct and reflected waves (Benson 1995; Neal 2004; Rodríguez-Abad et al 2011a).

Several references exist describing the use of GPR to assess material properties and examine the relationship between the real/imaginary relative permittivity and MC of wood. Martínez-Sala et al (2013) used GPR to assess physical properties of wood structures *in situ*. They contributed to the development of a GPR technique for studying the physical properties of timber. They found that the propagation velocities, as well as the amplitudes of the direct and reflected waves, were lower when the electric field was parallel to the grain rather than perpendicular. Although, in some cases, the reduction was small. Lorenzo et al (2010) demonstrated different applications of GPR in forestry. The 900-MHz and 1-GHz shielded antennas were used to obtain data in two different ways: with dynamic measurements (moving the antenna along the trunk or the timber) and static measurements. The preliminary measurements presented in their study indicate that the difference in the wave velocity or in the relative permittivity in living trees and in timber could be significant. Maï et al (2014) dealt with the study of the GPR technique for timber structure evaluation. They measured the dielectric relative permittivity using the resonance technique at 1.26 GHz on spruce and pine wood samples and using the geophysical survey systems, Inc. (GSSI, Nashua, NH) subsurface interface radar (SIR) 3000 system connected to a 1.5-GHz antenna on several wood samples. Their results showed that relationships exist between the real/imaginary relative permittivity and MC of the different wood samples. Moreover, GPR features in time domains present some correlations with the MC of wood material because of the dependence of wood permittivity on moisture. Hans et al (2015) investigated the MC of logs based on the propagation velocity (PV) of GPR signals. Linear regression between the log dielectric permittivity and MC was established for each of the investigated wood species (quaking aspen, balsam poplar, and black spruce), for the log state (thawed and frozen), and for the direction of measurement (on the log cross section [CS] and through the bark). Their results indicated that the models for quaking aspen and balsam poplar were similar to each other and differed from those of black spruce in terms of slopes and intercepts. Reci et al (2016) carried out a study of how moisture variations in wood materials affect the GPR signal. Results obtained by using direct waves in wide angle radar reflection configuration, in which one GPR antenna is moved whereas the other is in a fixed position, were compared with results obtained by using reflected waves in the so-called offset configuration in which the distance between GPR antennas is fixed. Overall, when the humidity level

increases, the difference between the permittivity values estimated by using the reflected and direct wave approaches increases. Rodríguez-Abad et al (2011b) used GPR with a 1.6-GHz antenna to show that significant differences existed in PVs, amplitudes, and spectra variations when the electromagnetic field was oriented parallel vs perpendicular to the grain (longitudinal vs radial or tangential). The differences observed when the field was oriented parallel to the radial axis vs the tangential axis (both are perpendicular to the grain) produced smaller differences than those between parallel and perpendicular to the grain.

Several scholars have explored the use of GPR on wood logs, wood structures, and other wood materials. Riggio et al (2014) summarized the test recommendations for selected NDT techniques as developed by members of the RILEM Technical Committee AST 215 "*in situ* assessment of structural timber." They demonstrated that GPR had several key advantages for assessing structural timber. GPR had the ability to identify common timber defects and excessive moisture, had good repeatability, and had low sensitivity to surface coupling. They also found that the method was not well suited for detecting thin defects. Colla (2010) performed laboratory tests of an ancient timber beam with the goal of evaluating the applicability and utility of using GPR in nondestructive inspection of existing timber structural elements. Halabe et al (2009) worked on precisely detecting the subsurface defects of wooden logs. SIR-20 with a central frequency of 900 MHz was used to test six hardwood logs. There was good correlation between the predicted defect locations and those found after examining sawed (CS) of the logs. The results from these tests showed that GPR had high accuracy in detecting subsurface defects such as subsurface metals, knots, and decay in wooden logs.

The potential of using GPR technology to inspect timber structures for internal defects has also been explored by other researchers. Cardimona et al (2000) performed GPR surveys over the driving lanes of 11 bridges and compared the deterioration analysis results with what ground truth was available. They obtained good correlation with the ground truth information showing that GPR could give accurate percentage deterioration estimates. The study demonstrated that GPR was effective by yielding deterioration estimates for key bridges in Missouri and described interpretation methodologies appropriate for high-resolution GPR imaging. Muller (2002) gave an overview of each of the techniques examined before focusing on the performance and potential applications for GPR in timber bridge inspection. In March-April 2002, a bridge was assessed using the NDT technique to locate internal defects in timber girders. Defect predictions were assessed by cutting CS from girders for inspection from the demolished bridge and by conducting a drilling investigation of the existing bridge. Of the techniques examined, GPR was found to be the most reliable method for locating internal defects. Pyakurel (2009) conducted research about assessing the possibility of detecting subsurface defects in logs using GPR before the sawing process. The study showed that the GPR-based system is suitable for use in timber saw mills to map hidden defects (eg knots and decays) and foreign objects (eg metallic nails) in wooden logs before sawing so that the yield of high-value defect-free lumber can be maximized. GPR can also be used as a rapid nondestructive tool to detect subsurface moisture, debonding, and monitoring the *in situ* condition of fiber-reinforced polymer composite–wrapped members.

Some researchers also conducted some studies using intelligent algorithms. Asadi et al (2019) proposed a novel machine learning–based processing for automatic interpretation and quantification of concrete bridge deck GPR B-scan images. The proposed approach provided a robust solution for automatic quantification of GPR field data after implementing a machine learning–based classifier and a fine-tuned filter. Alsharqawi et al (2018) proposed two enhanced models related to bridge deck condition assessment and deterioration modeling. A Weibull distribution function deterioration model was proposed which could function with relatively limited historical inspection data and stochastically capture the uncertainty and randomness of the deterioration process. The model provided the basis for

maintenance, repair, and replacement actions or the decision to delay intervention until a later time. Aguwa (2014) studied and structurally assessed the Nigerian grown Abura timber to understand its performance as timber bridge beams. The results indicated that Abura bridge beam depicted different safety levels when subjected to shearing forces under the various specified design conditions. Dinh et al (2018) presented an automated rebar localization and detection algorithm. The proposed methodology was based on the integration of conventional image-processing techniques and deep convolutional neural networks. The implementation of the proposed system in the analysis of GPR data for 26 bridge decks showed excellent performance. In all cases, the accuracy of the proposed system was greater than 95.75%. The overall accuracy for the entire deck library was found to be 99.60% $\pm$ 0.85%. Harkat et al (2019) demonstrated improved target localization and proposed an alternative classification methodology. A neural network radial basis function, designed *via* a multiobjective genetic algorithm (MOGA), was used to classify windows of GPR radargrams into two classes that are radargrams with or without target information. High-order statistic cumulant features were captured from samples. Feature selection was performed by MOGA, with an optional prior reduction using a mutual information approach. The obtained results demonstrate improvement of the classification performance.

MATERIALS AND METHODS

Visual Inspection

A unique set of aged timber highway bridges are located along a portion of the historic US Route 66 in Southern California. This stretch of historic Route 66 in the Mojave Desert is currently the focus of extensive efforts by the county of San Bernardino to preserve its iconic legacy and protect its key cultural and historical resources, which include the timber bridge structures (Wacker et al. 2017).

The Dola and Lanzit Ditch bridges, located approximately 10 km east of the city of Amboy, were the first two timber bridges to be deconstructed in March 2017. These bridges were built between 1930 and 1940 using untreated timber from naturally durable species. It has 5.8 m spans or multiple spans with stringers and a transverse

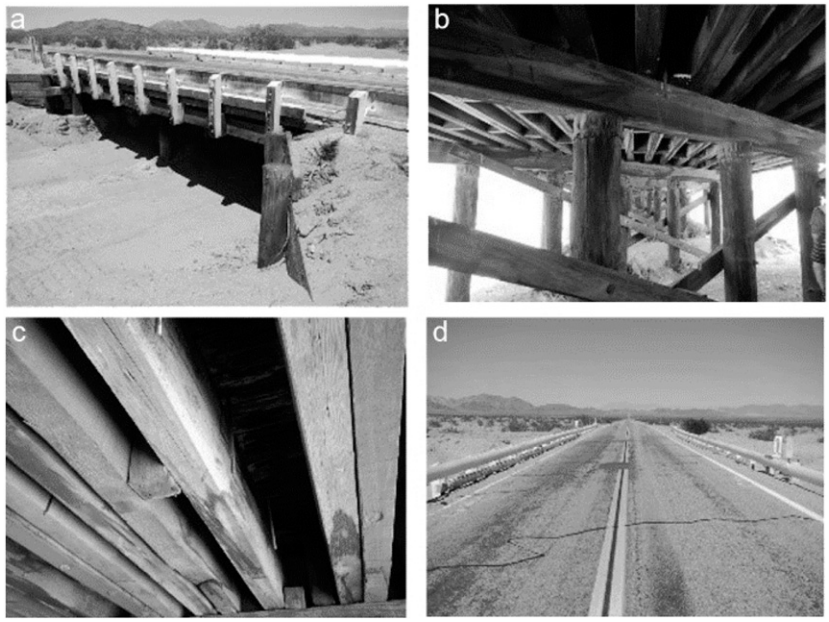

Figure 1. (a) Overview of the bridge structure, (b) underside view, (c) stringers, and (d) concrete deck with asphalt covering.

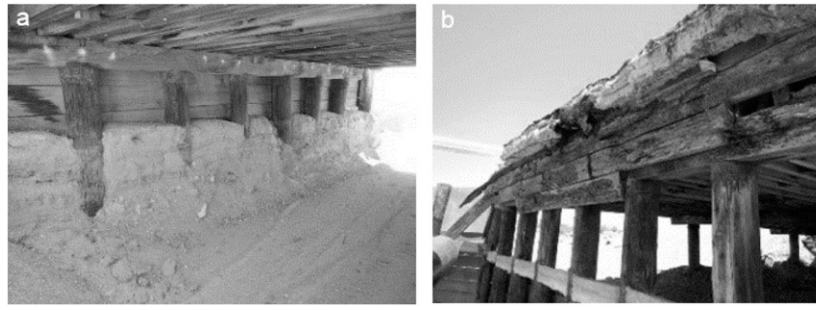

Figure 2. Bridge defects by visual inspection that include flood scouring: (a) annual floods deposited silt and (b) erosion around bridge abutments.

nail-laminated deck. After WWII, the bridge was widened. In the early 1950s, a concrete deck was added and then covered with asphalt (Fig 1).

Overtime, exposure to the environment has caused damage to the bridge and led to potential safety risks. Annual floods deposited silt (Fig 2[a]) under bridges and, in some cases, eroded bridge abutments (Fig 2[b]). The erosion also caused decay on the abutment back walls. Common methods of protecting and reinforcing the abutment include seasonal removal of silt, abutment wing wall repairs (Fig 3[a]), and adding temporary midspan shoring (Fig 3[b]). Damaged stringers were reinforced by attaching metal bars under the stringers. For the nail-laminated decks, repairs and regular evaluations of intermediate pier supports are also important (Fig 4[a] and [b]).

A visual inspection was conducted on each timber to document visible characteristics. Documentation included photographs and recording of feature locations for further NDT. Visual inspection identified external damage as shown in Figs 5 and 6. One common feature of the bridge timbers was holes for steel bars near the ends of the timber (Fig 5[a]). Along the length of the timbers were holes for steel connectors between the timber and the bridge structure; some of these holes contained nails broken during the disassembly process. Large splits and knots that extended to the surface were visible, but small or interior splits and interior knots cannot be located visually (Fig 6).

Data Collection

A combination of acoustic tomography, GPR, and microdrilling technologies were used for NDT at the selected CS. The results of the GPR are the focus of this report.

A total of 18 Douglas fir (*Pseudotsuga menziesii*) timbers were used in this study. Before testing, the beams were brought to a MC equilibrium of 10% in a temperature- and humidity-controlled

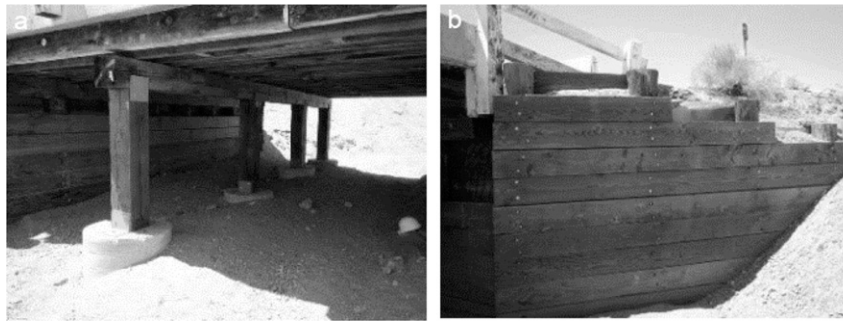

Figure 3. Protecting and reinforcing the bridge abutment: (a) midspan shoring and (b) wing wall repair.

Figure 4. Bridge evaluation: (a) reinforcement of damage stringers and (b) evaluation of intermediate pier pillars.

room. Specimen No. 7 was excluded from the study because it contained a series of cracks through the entire specimen, making it unsuitable for analysis. The labeling and scanning procedures for the timbers are shown in Fig 4. Each of the six faces of the timbers were given letters from A through F. Faces A and F were the ends of the timber. Scans started near Face A and continued along the sides toward Face F. Faces C and E had three scan lines each; Faces B and D had one scan line each. The distance between the scan lines on Faces C and E was 9.5 cm. The center scan line for Faces C and E was along the midline of the face. A total of 68 lines were scanned for the 17 timbers. The GPR produces a B-scan image along each scan line. The GPR unit in this study was a SIR System-4000. The instrument was manufactured by GSSI with a 2-GHz palm antenna as shown in Fig 7. Acoustic testing data were collected along the same lines used for GPR scanning. The acoustic evaluation tool in this study was a Fakopp acoustic device, which measures the time of flight (TOF).

The timbers were placed on two sawhorses. The scanning lines shown in Fig 8 were marked on the faces using a chalk line and blue marking chalk. The 2-GHz palm antenna, shown in Fig 7(a), was placed at the start of the line. The beam was rotated so that the side to be scanned was horizontal and facing upward for ease of access. The antenna has

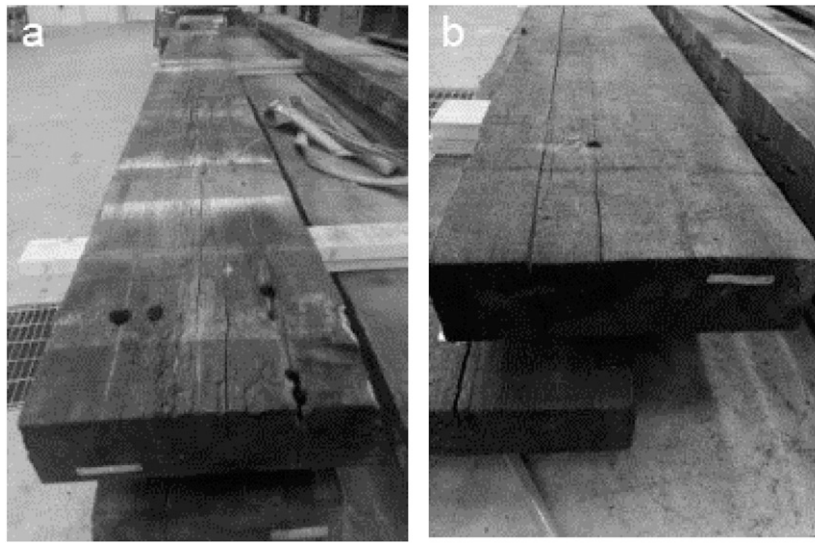

Figure 5. Common defects of timbers: (a) holes of metal bars and (b) cracks and splits on the timber surface.

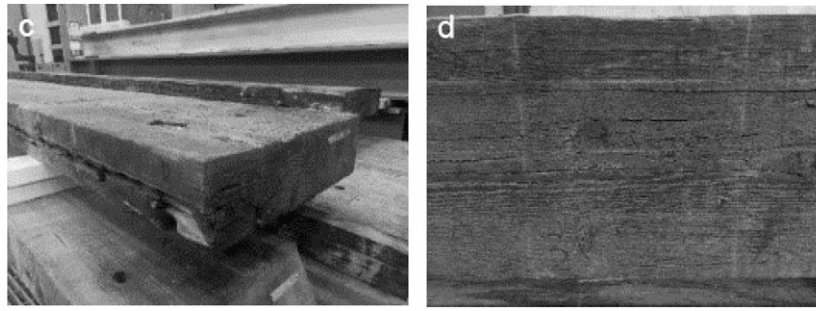

Figure 6. Common defects of timbers: (a) drilled holes and bar holes with some cracks and (b) visible surface knots.

the capability of placing marks on the radargram while scanning is underway. This mark does not interfere with data collection and is a tool to indicate a point of interest during later analysis. Marks were placed at 0.3-m intervals to aid in locating features. The antenna transmitted the electromagnetic wave used in the scan and received the reflected waves from the scanned object. The GPR operational parameters were kept constant during inspection. Figure 9(a) shows the scanning environment. For the acoustic tests, probes were driven into the surface of the timber along the scan lines at distances of 0.3 m as shown in Fig 9(b). The acoustic scan locations corresponded to the locations marked on the radargrams using the antenna. One probe was struck to produce a mechanical stress wave, and the other probe received the stress wave. The time between the first probe being struck and the second probe receiving a signal was measured by the Fakopp unit and displayed as the TOF of the wave. To obtain consistent TOF values at each location, the measurement was performed five times. The first two seated the probe firmly. The last three were recorded and averaged for TOF values. Last, the location, size, and nature of visible surface defects were recorded as shown in Fig 10. This process is referred to as defect mapping in this report.

GSSI Setup before Test

The dielectric constant is an expression of the ratio of permittivity of a substance to permittivity in vacuum. It describes how quickly an electromagnetic wave generated by GPR travels through materials. Materials that have low dielectric values allow radar to propagate more quickly than materials with high dielectric values. The dielectric values of the timbers are determined by placing a reflective metal bar on the side of the timber opposite to the antenna. The metal bar is readily visible on the GPR output screen. Because the GPR is recording the time necessary for the electromagnetic wave to reflect off an object and return to the antenna, the distance to the object can

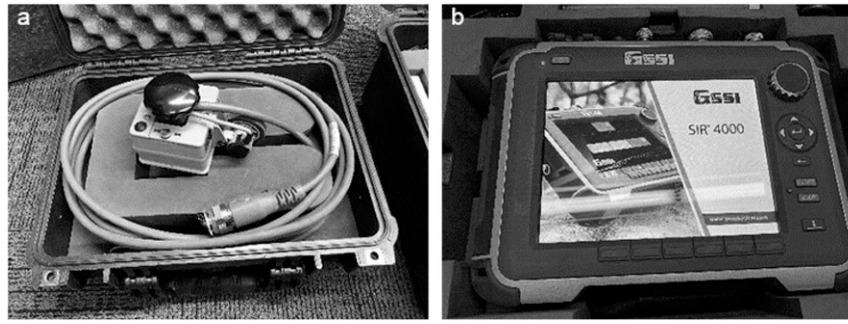

Figure 7. Ground- penetrating radar test equipment: (a) probe and (b) data collection module.

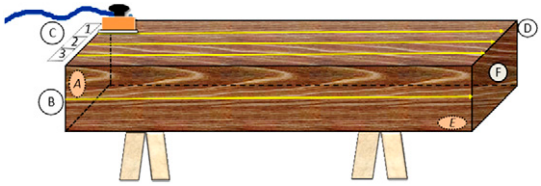

Figure 8. Ground- penetrating radar scanning setup. Scans start near face A and end near face F. Faces C and E have three scan lines each that are spaced 9.5 cm apart. The single scan line on Faces B and D are always along the middle of the face.

be determined by multiplying the travel time of the wave by the speed of the wave. Conversely, if the distance to the object is known, then the assumed dielectric constant of the wood can be adjusted within GPR software such that the reported distance matches the known distance between the antenna and the object. In this way, the dielectric constant of each timber was determined. The control settings of the SIR-4000 GPR unit used during testing are given in Table 1 (GSSI 2014).

Processing of GPR Data (in software)

RADAN 7 software (GSSI, Nashua, NH) was used to process the GPR radar grams used this software to process the scanned data from the experimental samples. The data file includes raw data and data with signal gain. Several processing techniques, which are built into RADAN 7 software, were applied to the data. Parallel bands observed in the scans were the result of plane reflectors such as the ground surface, soil horizons, and bands of low frequency noise (Butnor et al 2003) and are shown in Fig 11. Consistent bands that ran the length of the radargram were removed using the "background removal" filtering technique. Often, defects appeared to have hyperbolic tails in the radargrams. These tails were an artifact of the scanning process. A filtering technique referred to as "migration" removes these tails by collapsing the hyperbolic diffractions and provides a better estimation of the location of the feature within the timber. The migration technique used in this study is built into RADAN 7 software and is based on Kirchoff migration, which identifies the geometry of the hyperbolic reflector and reduces the impact of multiple reflections (Hogan 1999; Yao and Wang 2012).

RESULTS AND DISCUSSION

The scanning tests were conducted on each side to provide data to develop a three-dimensional visualization of the timber. The collected information complements the data collected

Figure 9. Testing environment: (a) radar test environment and (b) acoustic testing environment.

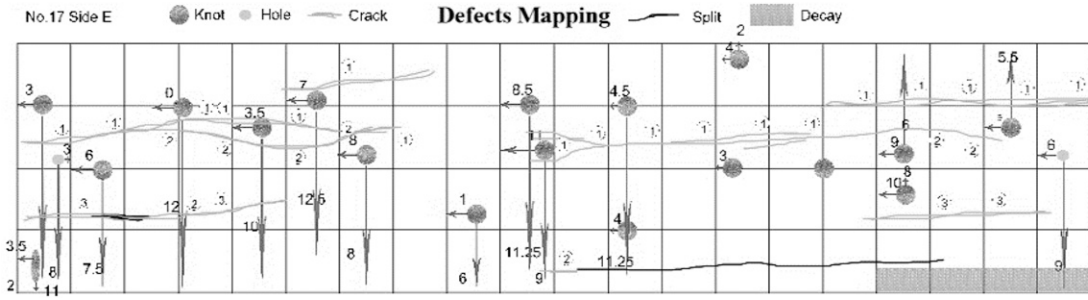

Figure 10. Defect mapping.

through visual inspection. The number of characteristics identified through visual inspection of the timbers are given in Table 2 and Fig 12. Characteristics include decay, breaks, cracks, holes, knots, steel bars, steel nails, and fixed plates. Among the 18 timbers, No.7 was unsuitable for the radar test because of the presence of a break through the entire length of the timber. The radargrams revealed some timbers with greater numbers of particular defects. Among them, four timbers (Nos. 5, 9, 17, and 18) had the highest numbers of cracks, knots, holes, and steel nails. The information from the acoustic tests supports the radargram identification of defects within the timbers. Timber No. 5 had the highest number of holes (38) distributed across four sides. In addition, 64 cracks were present. Timber No. 9 had the highest number of cracks (86) and a high number of knots (37). Timber No. 17 had the highest number of knots (52) and a high number of cracks (72). Timber No. 18 had 105 steel nails scattered along the top side. In addition to GPR scans, acoustic tests, and field visual inspections, photographs recorded the locations of the characteristics along the timbers. There were 25 cracks, 14 knots, 38 holes, and 44 nails or bars visible on the surface of the timbers. Different visible features can be found in the radargrams. The condition of two sides, Faces C and D, on No. 5 is shown in Fig 13. Comparing the defect-mapping data, the photographs, and the GPR images is a valuable way to locate defects. They clearly and accurately reflect the visible condition. The highlighted reflected waves inside the red square (Fig 13[c]) are between 12.7 cm to 177.8 cm and 279.4 cm to 431.8 cm, and correspond to cut sample No. 1 (Fig 13). They can be detected on the three-dimensional image as shown in Fig 13(e).

There are also many nails that cannot be seen because of a small diameter or short length. Nails and bars were used to connect the bridge components. When the bridge was dismantled, several holes were left by the removal of the

Table 1. Control settings used on the subsurface interface radar-4000 unit.

Radar-parameter	Setting/value	Process parameter	Setting/value
Collect model	Distance mode	Gain model	Manual
Scans/second	200	Edit gain curve	8 points
Samples/scan	512	FIR low pass	4000 MHz
Scans/in	10.0	FIR high pass	500 MHz
In/mark	120.0	FIR stacking	Off
Soil type	Custom	FIR BG removal	0
Time range	3.00 ns	IIR low pass	Off
Position model	Manual	IIR high pass	10 MHz
Offset	11.90	IIR stacking	0
Surface	0%	IIR BG removal	0
		Signal floor	Off
		Filters	Off

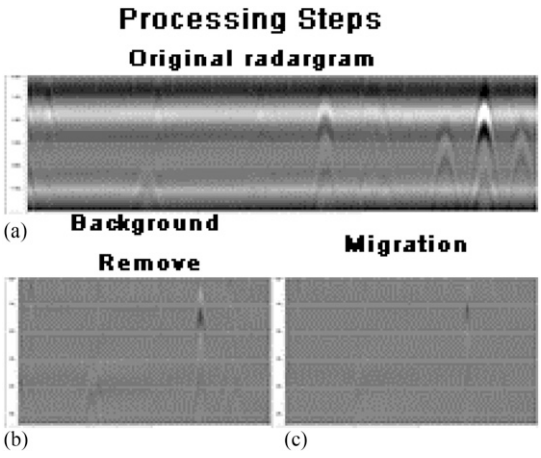

Figure 11. Processing steps in the data file: (a) raw data from an SIR4000 ground- penetrating radar system with a 2-GHz palm antenna. Clear reflected waves were shown and also some noises; (b) radargram processed in RADAN 7 software after the background removal step. The background noises such as the black and white parallel area in (a) were removed based on the visual observation; (c) using background removal and Kirchoff migration, the tails of reflected waves were removed by collapsing the hyperbolic diffractions. The locations of the features were better estimated.

connections. The relatively dark and fuzzy areas on the radargrams (Fig 13[c] and [d]) shown within the white squares were verified as holes by comparing the defect mapping with the photographs. These findings correspond with the cut sample No. 2 in Fig 13. The yellow boxes indicate knots detected by the GPR. The presence of knots is verified in cut sample No. 3 in Fig 13.

During disassembly of the bridge, the process of withdrawing connecting bars and nails sometimes caused splits and cracks to appear. Hairline cracks and splits are difficult to detect with GPR. Because the GPR wave is reflected at interfaces of different dielectric constants, only cracks and splits sufficiently wide to have an air gap between the opposite sides of the defect will be detected. The long split shown in Fig 13(b) is sufficiently wide to reflect the wave; it is visible in Fig 13(d) and marked with a dashed blue line. A closer view of the split is shown in cut sample No. 4. At this time, internal defects can be located within the radargrams, but they cannot be characterized using only the radargram. Also, determining the defect size can be challenging using a 2D image.

RADAN software allows abutting 2D images to be assembled into a 3D image. The 3D image gives additional information regarding the size and location of defects. The compiled 3D image is shown in Fig 14(a); the yellow lines show the outline of the timber, and the bright areas are the interior metal. As mentioned in the description of Fig 8, the sides of the timbers were scanned along three lines using both GPR and acoustic stress wave inspection. The

Table 2. Defect statistics on 18 timbers.

No.	Decay	Break	Crack	Knot	Hole	Steel bar/nails	Fixing plate	Fixing nail	Split
1	0	0	10	7	25	68	2	17	0
2	1	0	36	5	10	5	2	0	1
3	0	0	0	21	5	18	0	0	25
4	0	0	26	14	14	17	0	0	0
5	0	1	25	14	38	44	0	0	0
6	0	0	10	10	19	57	1	9	0
7	0	0	0	0	0	0	0	0	0
8	0	0	14	37	4	23	0	0	0
9	0	0	20	37	2	11	0	0	0
10	3	0	27	27	18	43	0	0	0
11	1	2	16	48	21	29	0	0	5
12	1	1	10	24	3	86	0	0	3
13	1	6	6	10	28	67	2	10	4
14	0	1	0	29	7	67	0	0	4
15	0	0	17	12	18	32	2	16	2
16	2	0	10	23	23	78	0	0	10
17	0	3	24	52	23	26	0	0	24
18	2	0	4	23	7	105	0	0	0

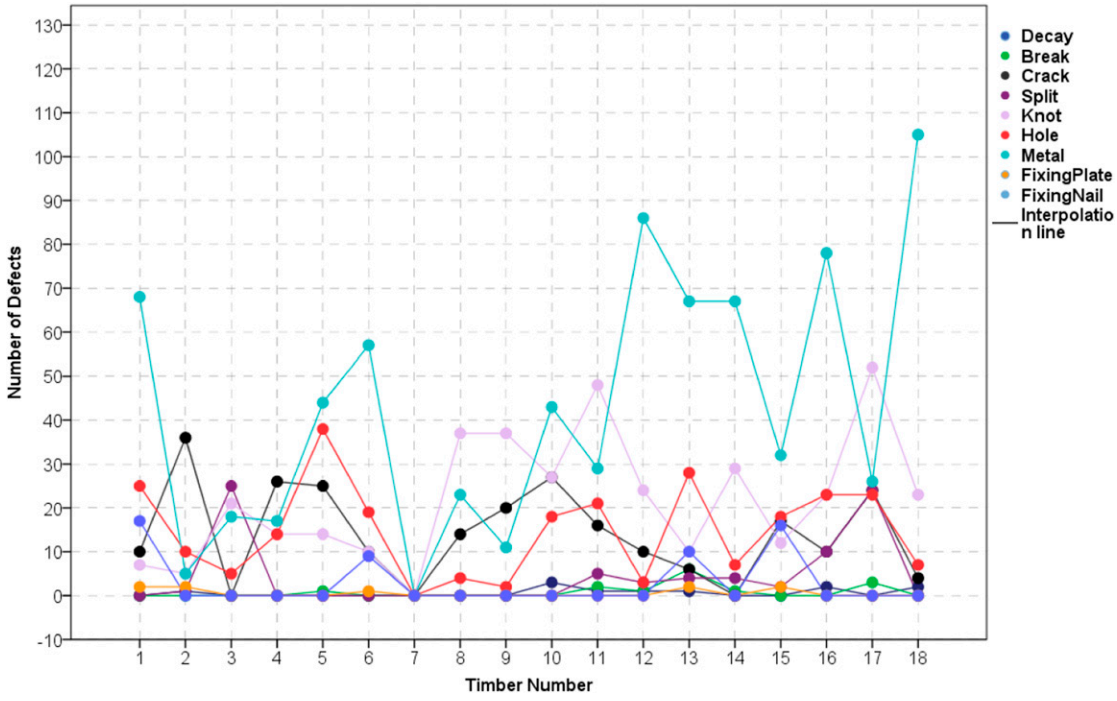

Figure 12. Defect account of 18 timbers.

results of the acoustic inspection are shown in Fig 14(b). Higher microsecond travel times from 1.23 m to 2.13 m and 4.57 m to 5.80 m are seen in areas of metal connectors as identified by the 3D GPR scan in Fig 11(a). The higher microsecond travel times also reflected the split as shown in Fig 13(b). The higher travel times may be caused by the presence of the metal connectors or damage

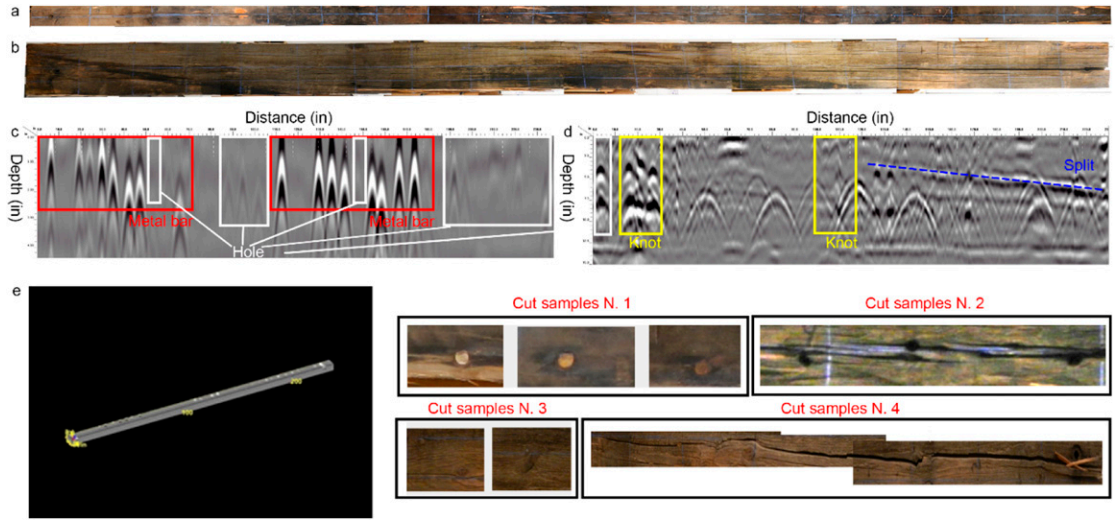

Figure 13. Comparison of No. 5 timber with radargram and camera pictures.

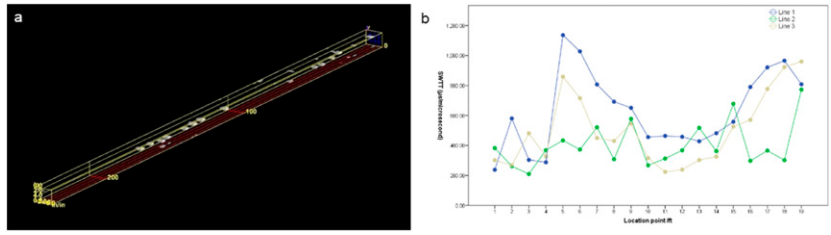

Figure 14. 3D and acoustic results of No. 5: (a) 3D image of No. 5 and (b) the results of acoustic tests.

to the wood surrounding the connectors caused by the disassembly process. The combination of the photographs and the acoustic stress wave inspections provides verification of the GPR results.

Timber 18 had many defects: four cracks, 23 knots, 7 holes, and 105 metal nails and bars. Figure 15(a) and (b) show Faces D and E. Surface defects were identified from the images. Metal connectors were used along the length Face D of the timber. The connectors were driven perpendicular to Face D and parallel to Face E. Scans of Face E show high numbers of metal connectors; the connectors are identified by red boxes in Fig 15(c). The white dots in the 3D image shown in Fig 15(e) correspond to the locations of the metal connectors. The nails are shown in cut sample No. 1. Several bars were used to assemble the bridge. The Face D scan revealed two large bars indicated by red boxes in Fig 15(d). During disassembly, many of these bars were removed leaving holes; these holes are shown in Fig 15(d) within the white boxes. Large knots are also visible and are identified with yellow boxes. A close-up view of the knots is shown in cut sample No. 3. The black box in Fig 15(b) and the black line in Fig 15(d) indicate a region of decayed and broken wood. A larger view of the decayed region is shown in cut sample No. 4. Reflections caused by metal are noticeably brighter than reflections caused by other features. Smaller diameter nails produce less noticeable reflections than larger diameter nails. In some cases, closely spaced metal connectors appear as a single feature in the radargram.

The 3D perspective image constructed from Face D scans shown in Fig 16 allows an overall

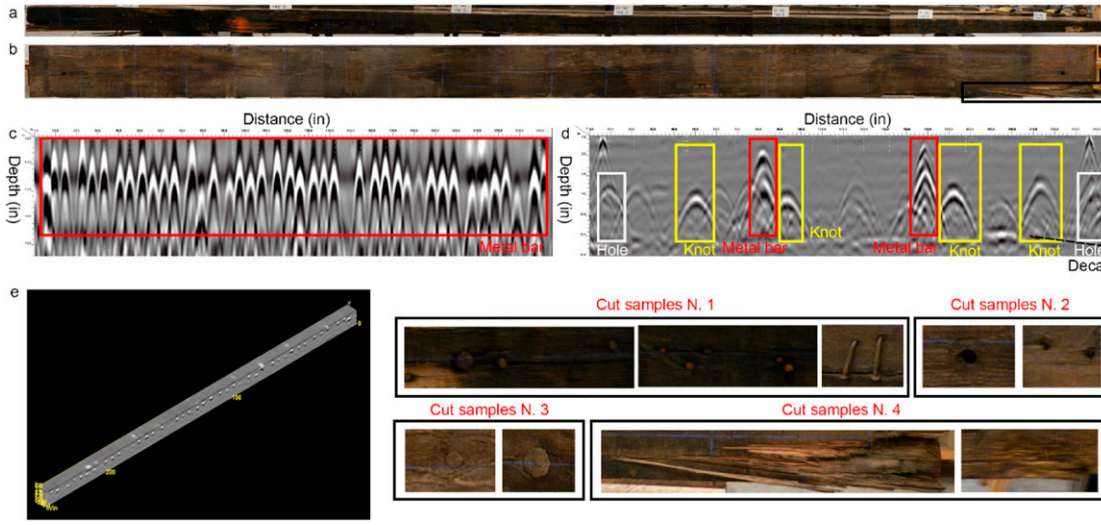

Figure 15. Comparison of No. 18 timber with radargram and camera pictures.

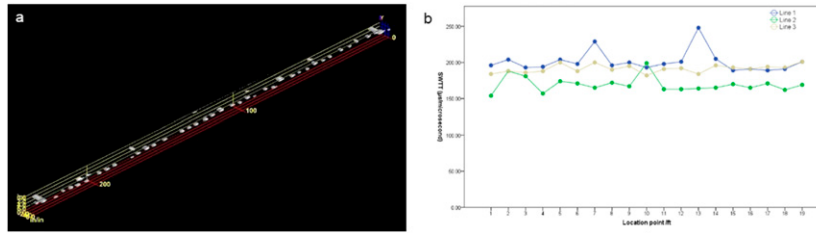

Figure 16. 3D and acoustic results of No. 18: (a) 3D image of No. 18 and (b) results of acoustic tests.

assessment of the timber. The white regions indicate metal connectors. The results of the acoustic stress wave tests are shown in Fig 16(b). Two notable regions of higher TOF are between 1.83 m to 2.44 m and 3.66 m to 14 ft 4.27 m. These regions correspond to the metal bars shown in the red boxes of Fig 16(d).

CONCLUSIONS

This article presents a multidisciplinary evaluation performed on timbers from a bridge located on a portion of Route 66 in Southern California. Nondestructive methods were used to assess the timbers. In this context, GPR provided a valuable contribution to the assessment of the wood structures. GPR tests identified the location and size of the defects and distinguished between some categories of defects. According to the GPR results, 0.8-cm-diameter metal bars were easily visible, whereas 0.5-cm-diameter metal nails were unclear. Common knots on the timber surface were relatively darker than the waves reflecting off metal bars when the diameter of the knot was greater than 1.9 cm. Decayed and broken wood existed in the same area. In addition, the presence of cracks and splits usually resulted in a high microsecond value, and these were detected in the radargrams when the width of the crack or split was greater than 0.4 cm. GPR allows accurate nondestructive evaluation of wood timbers by reliably identifying the location of internal features. Metal features are prominent and easy to characterize. Cracks and splits must be of a sufficient width to be detected. Although both knots and holes can be located by GPR, they cause similar types of features to appear within the radargrams, making them difficult to differentiate.

ACKNOWLEDGMENTS

This article describes a laboratory study conducted by the USDA Forest Service, Forest Products Laboratory, in cooperation with the county of San Bernardino (California) and Biggs Cardosa Associates, Inc. The authors would like to acknowledge the contributions of Xiaoquan Yue, lecturer, Fujian Forestry Agriculture and Forestry University, Fuzhou, Fujian, China, and Fenglu Liu, PhD student, Beijing Forestry University, Beijing, China, for their assistance in data collection. Also, the staff of the USDA, Forest Service, Forest Products Laboratory, Engineering Mechanics and Remote Sensing Laboratory, for their assistance in preparing specimens for testing during this laboratory study. Financial support to Xi Wu's visiting study in the United States was provided by the China Scholarship Council.

REFERENCES

Aguwa JI (2014) Structural performance of the Nigerian grown Abura timber bridge beam subjected to compression and shearing forces. KSCE J Civ Eng 19(4):974-981.

Alsharqawi M, Zayed T, Dabous SA (2018) Integrated condition rating and forecasting method for bridge decks using visual inspection and ground penetrating radar. Autom Construct 89:135-145.

Asadi P, Gindy M, Alvarez M (2019) A machine learning based approach for automatic rebar detection and quantification of deterioration in concrete bridge deck ground penetrating radar B-scan images. KSCE J Civ Eng 23(6): 2618-2627.

Benson AK (1995) Applications of ground penetrating radar in assessing some geological hazards: Examples of groundwater contamination, faults, cavities. J Appl Geophys 33:177-193.

Butnor JR, Doolittle JA, Johnsen KH, Samuelson L, Stokes T, Kress L (2003) Utility of ground-penetrating radar as a root biomass survey tool in forest systems. Soil Sci Soc Am J 67(5):1607.

Cardimona S, Willeford B, Wenzlick J, Anderson N (2000) Investigation of bridge decks utilizing ground penetrating radar. *In* International Conference on the Application of Geophysical Technologies to Planning, Design, Construction, and Maintenance of Transportation Facilities, December 11-15, 2000, St. Louis, MO.

Colla C (2010) GPR of a timber structural element. Pages 1-5 *in* Proc. XIII International Conference on Ground Penetrating Radar, IEEE, Lecce, Italy.

Dinh K, Gucunski N, Duong TH (2018) An algorithm for automatic localization and detection of rebars from GPR data of concrete bridge decks. Autom Construct 89:292-298.

Geophysical Survey Systems, Inc (2014) SIR 4000 manual. Geophysical Survey Systems, Inc., Nashua, NH. https://www.geophysical.com/wp-content/uploads/2017/10/GSSI-SIR-4000-Manual.pdf.

Halabe UB, Agrawal S, Gopalakrishnan B (2009) Nondestructive evaluation of wooden logs using ground penetrating radar. Nondestruct Test Eval 24(4):329-346.

Hans G, Redman D, Leblon B, Nader J, Larocque A (2015) Determination of log moisture content using ground penetrating radar (GPR). Part 2. Propagation velocity (PV) method. Holzforschung 69(9):1125-1132.

Harkat H, Ruano AE, Ruano MG, Bennani SD (2019) GPR target detection using a neural network classifier designed by a multi-objective genetic algorithm. Appl Soft Comput 79:310-325.

Hogan G (1999) Migration of ground penetrating radar data: A technique for locating subsurface targets. SEG Tech Prog Exp Abstr 7(1):1359.

Lorenzo H, Pérezgracia V, Novo A, Armesto J (2010) Forestry applications of ground-penetrating radar. For Syst 19(1):5-17.

Maï T, Sbartaï Z, Bos F, Razafindratsima S, Demontoux F (2014) Non-destructive evaluation of timber structures using GPR technique. Pages 218-222 *in* 15th International Conference on Ground Penetrating Radar, IEEE, Brussels, Belgium, June 30-July 4, 2014.

Martínez-Sala R, Rodríguez-Abad I, Diez Barra R, Capuz-Lladró R (2013) Assessment of the dielectric anisotropy in timber using the nondestructive GPR technique. Constr Build Mater 38:903-911.

Muller W (2002) Trial of ground penetrating radar to locate defects in timber bridge girders. *In* State Conference, Institute of Public Works Engineering Australia (IPWEA) Queensland Division, Noosa Lakes Convention Centre, October 6-10, 2002, Queensland, Australia.

Neal A (2004) Ground-penetrating radar and its use in sedimentology: Principles, problems and progress. Earth Sci Rev 66(3-4):261-330.

Novo A, Solla M, Montero-Fenollós JL, Lorenzo H (2014) Searching for the remains of an Early Bronze Age city at Tell Qubr Abu al-'Atiq (Syria) through archaeological investigations and GPR imaging. J Cult Herit 15:575-579.

Núñez-Nieto X, Solla M, Novo A, Lorenzo H (2014) Three-dimensional ground-penetrating radar methodologies for the characterization and volumetric reconstruction of underground tunneling. Constr Build Mater 71:551-560.

Pyakurel S (2009) Two-dimensional and three-dimensional GPR imaging of wood and fiber reinforced polymer composites. PhD dissertation in Civil and Environmental Engineering, West Virginia University, Morgantown, WV.

Reci H, Maï TC, Sbartaï ZM, Pajewski L, Kiri E (2016) Non-destructive evaluation of moisture content in wood using ground-penetrating radar. Geosci Instrum 5(2):1-12.

Riggio M, Anthony RW, Augelli F, Kasal B, Lechner T, Muller W, Tannert T (2014) *In situ* assessment of structural timber using non-destructive techniques. Mater Struct 47(5):747-766.

Rodríguez-Abad I, Martínez-Sala R, Capuz R, Díez R, García F (2011a) Assessment of the variation of the moisture content in the *Pinus pinaster* Ait. using the non destructive GPR technique. Mater Constr 61(301):143-156.

Rodríguez-Abad I, Martínez-Sala R, García F, Capuz-Lladro R, Díez R (2011b) Non-destructive characterization of maritime pine sawn timber dielectric anisotropy by means of GPR. Pages 1-5 *in* 2011 6th International Workshop on Advanced Ground Penetrating Radar (IWAGPR), June 22-24, 2011, Aachen, Germany.

Wacker J, Mikhail M, Dizon G (2017) Evaluation of bridge components salvaged from historic Route 66 in California. Research in Progress RIP-4719-038. USDA Forest Service, Forest Products Laboratory, Madison, WI.

Yao Q, Wang QF (2012) Kirchoff migration algorithm for ground penetrating radar data. Pages 396-398 *in* International Conference on Computer Science & Electronics Engineering, IEEE, March 23-25, 2012, Hangzhou, China.